International Journal of Fracture **55**: 47–63, 1992.

Process region changes for rapidly propagating cracks

ERLAND JOHNSON
Division of Solid Mechanics, Lund Institute of Technology, Box 118, S-221 00 Lund, Sweden

Received 1 June 1991; accepted 23 September 1991

Abstract. A finite element model of a plate, which contains an initial crack subjected to a rapid loading at its faces, is investigated. A cell model of the prospective process region is adopted. The cell size is assumed to represent some characteristic intrinsic material length. The size of the process region is not predetermined but depends at every time on the number of cells that have reached a state characteristic for the process region i.e. essentially instability if load control would prevail. Outside the process region the material is assumed to be linearly elastic.

For low loading magnitudes the simulations show a rather long period of crack acceleration, but at higher loads this period is short or even not detectable, and a constant terminal velocity, significantly lower than the Rayleigh wave velocity, is reached. At lower loads both the energy release rate and the extension of the process region stay rather constant, but at higher loads they increase considerably with time, even though the crack tip velocity stays constant. Thus it appears that a tendency towards increased energy flow to the process region is met by increased size of this region, and thereby increased energy dissipation per unit of crack growth, rather than by increased crack edge velocity. The process region may finally occupy several cell rows, and the control of the process region by the characteristic length is thus lost. This can explain the apparent loss of the unique relation between stress intensity factor and crack edge velocity at high crack velocities.

In some simulations branching was obtained. The results from the simulations showed qualitative agreement with some recent experimental results e.g. those by Ravi-Chandar.

1. Introduction

Griffith [1] and Irwin [2] assumed that crack growth at small scale yielding occurred under constant energy release rate, specific for each material and environmental condition (such as temperature). It was later taken for granted that the small scale yielding energy release rate at dynamic crack growth could be represented by a unique function of the crack tip velocity for each material. Several experiments, first those by Paxson and Lucas [3], indicated that such a function could show a very strong dependence on the crack tip velocity.

In an attempt to theoretically explain results such as those by Paxson and Lucas, Broberg [4] argued that the process region could be considerably larger at high velocities than at low ones. This could explain the strong velocity dependence, but as a consequence a material-related length parameter, which controls the size of the process region at low crack tip velocities, loses its ability to do so at very high velocities. Such a loss removed the basis for the theoretical conclusion that the small scale yielding energy release rate was a unique function of the crack tip velocity for each given material [4, 5]. This conclusion was supported by experiments performed by Ravi-Chandar [6], Ravi-Chandar and Knauss [7, 8, 9, 10], Kalthoff, Winkler and Beinert [11] and Kalthoff [12] which apparently confirmed that dynamic crack growth at small scale of yielding could proceed under different energy release rates at the same crack tip velocity. In several experiments a surprisingly constant velocity could prevail even though both direct measurements and theoretical calculations showed considerable variation of the energy release rate. This seems to indicate that a tendency towards increased energy flow to the crack tip region results in a larger process region rather than an increased crack edge velocity.

Figures 1 and 2 show results adapted from Ravi-Chandar [6], also reported in [9]. For the lowest velocity the energy release rate $\mathcal{G}$ to the crack edge appears to be approximately constant at constant velocity, whereas it varies quite remarkably at a constant high velocity.

The present work is an attempt to explain the apparent fact that there is no unique relation between small scale yielding energy release rate and crack tip velocity in the high velocity region. The basis for this work consists of an assumption that the size of the process region is not predetermined. A cell model of the material, (cf. [4] and [13]), is therefore adopted and the size of the process region depends on the number of cells per unit of crack growth that reach a state characteristic to a process region, i.e. essentially instability if load control would prevail. Ideally each cell should correspond to a material volume that contains one nucleus for micro-separation, for instance an inclusion. However, the model would then contain a very large number of cells, perhaps 10^5–10^6, to cover the whole succession of prospective process regions in a material of the kind used in the experiments referred to. For computatonal reasons only a much smaller number, less than 10^4, can be handled and therefore a material modelled with a much coarser cell structure had to be chosen.

Since the main hypothesis concerns the role of the process region, an accurate modelling of the continuum outside this region does not appear to be necessary. For simplicity, therefore, the continuum is assumed to be linearly elastic.

During the course of the investigation it was, quite unexpectedly, found that branching or attempts to branching resulted in some of the simulations. Attempts to branching were found quite frequently on a micro-structural scale. This is in agreement with several investigations, among them those by Ravi-Chandar [6] and Ravi-Chandar and Knauss [9] who found that several branching attempts preceeded successful branching. This was also assumed by Pärletun

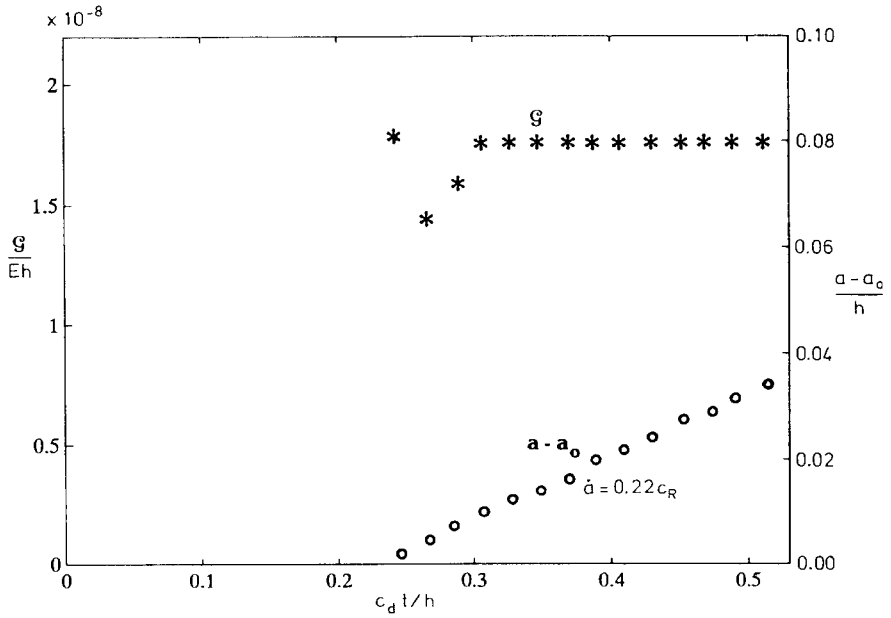

Fig. 1. The energy release rate $\mathcal{G}$ and crack length increment $a-a_0$ against time for a low loading magnitude; adapted from results by Ravi-Chandar [6]. Young's modulus is E, the length of the specimen is h (cf. Fig. 3). c_d denotes the longitudinal wave velocity in a thin plate. The crack velocity is $\dot{a} = 0.22c_R$ where c_R is the Rayleigh wave velocity in a thin plate. The result is interrupted at $c_d t/h \approx 0.53$. At this time stress waves, reflected at the boundaries, reach the crack tip.

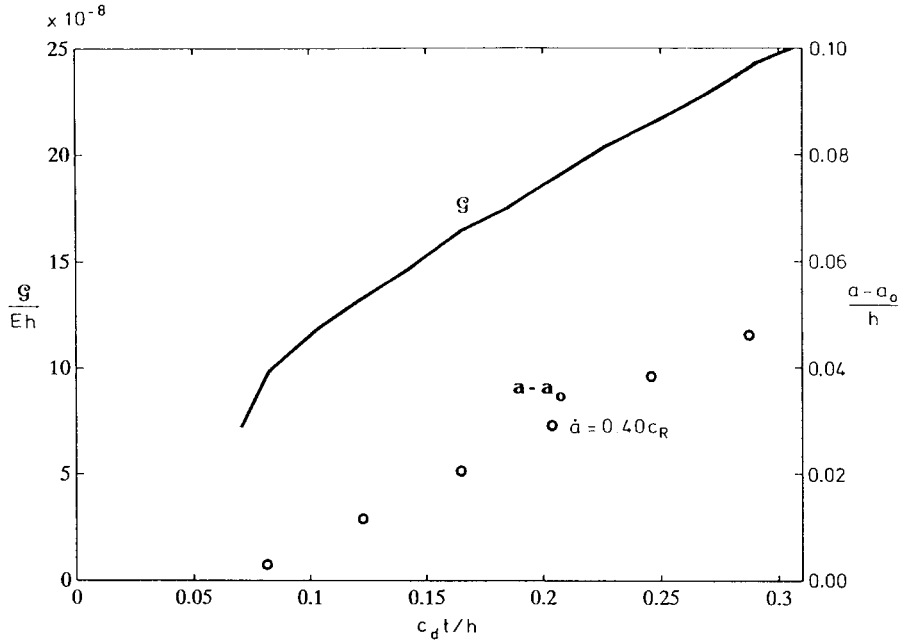

Fig. 2. The energy release rate $\mathcal{G}$ and crack length increment $a-a_0$ against time t for a high loading magnitude; adapted from results by Ravi-Chandar [6]. The crack velocity is $\dot{a} = 0.40c_R$. The crack propagation is recorded for times $c_d t/h \leqslant 0.31$. Thus it is terminated before the interaction of waves reflected at the boundaries. The result for the energy release rate is shown as a solid line since no data points are presented in the original work [6].

[14], who attributed unsuccessful branching to the apparent fact that the shorter of two micro-structurally small branches is quickly arrested except at very high crack tip velocities. In the present investigation this result could not be simulated, since perfect symmetry is inherent in the model.

2. The model

2.1. Geometry and loading

A plane stress model is used. The geometry, shown in Fig. 3, corresponds to that used by Ravi-Chandar [6] and Ravi-Chandar and Knauss [7], [8], [9] and [10] in their investigations of rapid crack propagation in Homalite 100. An initial crack of length a_0 is prepared and a constant pressure p is reached at its faces after a rise time of $c_d t/h \approx 0.10$. The length of the specimen is h and its height is $2b$. By appropriate choices of a_0/h and b/h, it is possible to avoid waves, generated by the pressure application at the crack faces and reflected from the boundaries, to interact with the crack within a comparatively long time of simulation. During this interval the geometry is thus equivalent to an infinite geometry. In the simulations Poisson's ratio $\nu = 0.31$ (as for Homalite 100), $a_0 = 0.60h$ and $b = 0.30h$. This implies that longitudinal waves travelling with velocity c_d and reflected from the upper (or lower) boundary will reach the crack tip at a normalized time $c_d t/h \geqslant 0.60$ while longitudinal waves reflected at the right edge will arrive at $c_d t/h \approx 0.52$ if the crack at all times propagates with the Rayleigh wave velocity. Thus the latter value is a lower limit to the time during which the geometry can be regarded as

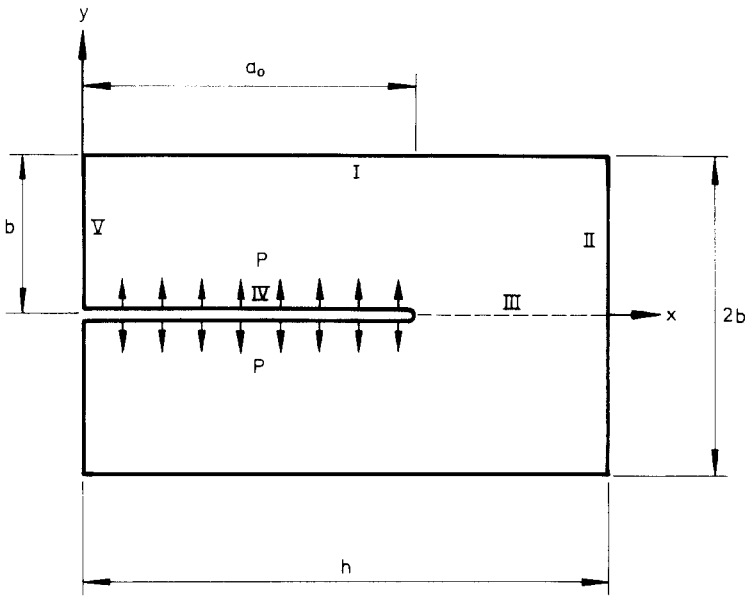

Fig. 3. The geometry used by Ravi-Chandar [6] in his investigations of rapid crack propagation in Homalite 100. Due to the symmetry only the upper half with boundaries *I*, *II*, *III*, *IV* and *V* is used in the simulations. The initial crack length is a_0, the height is $2b$ and the length is h. In the experimental results presented $a_0 \approx 0.63h$ and $b = 0.30h$. The same b-value is used in the simulations while an initial crack length $a_0 = 0.60h$ is used. The crack surfaces are loaded by a pressure p, which is constant after a rise time $c_d t/h = 0.03$.

infinite. In each specific experiment or simulation this time can, of course, be accurately determined. The value $a_0 = 0.60h$ differs somewhat from the value $a_0 \approx 0.63h$ used by Ravi-Chandar [6]; this difference, however, is unimportant as long as no reflected waves have reached the crack tip.

2.2. *Material behaviour in the process region*

The material in the near-tip region is assumed to possess a large number of sites where nucleation of defects occurs. Restriction is made to the case where only one type and size of defect dominates. The nucleation sites are homogeneously distributed over the specimen and they all have the same excitability. The specimen is divided into cells in the prospective process region (the region where the influence from the defects on the material behavior is expected to be noticeable). Due to the unrealistically large computer times otherwise expected, the cells have to be chosen far too large to represent a real material as mentioned above. However, even though the linear dimensions of the cells are perhaps a factor 100 or more too large, the model is expected to catch the main phenomena that are due to the influence from a characteristic material length in the prospective process region. Each cell is assumed to contain one main defect. When the relative volume increase v of the cell reaches a critical value $v = v_1$ the cell response will change from the linearly elastic one to one that would lead to instability under load control. Thus cell softening starts abruptly when v reaches the value v_1. Nucleation is thus not specifically taken into account. When the critical volume is reached, the defects are assumed to grow with increasing cell volume independently of the rate of volume increase. This growth of the defects weakens the cells. No dependence of displacement biaxiality is taken into account.

Therefore only one parameter ω is needed to characterize the weakening behaviour. This is accomplished by inclusion of ω as a factor in the cell stiffness. When the relative volume v increases from v_1 to v_2, parameter ω decreases from 1.0 to 0.0 according to

$$\omega(v) = \frac{(v_2/v)^n - 1}{(v_2/v_1)^n - 1}. \tag{1}$$

For $v \geqslant v_2$ the parameter ω remains zero. This corresponds to a cell with zero stiffness and thus a cell which can be disregarded in the future: it will be said to have vanished. If the cell volume for some reason decreases after some amount of softening, the current ω-value is maintained until the previous maximum volume again is reached. Then softening continues according to (1). Unloading is thus explicitly taken into account.

The finite elements are modelled as cells in the 12 element rows closest to the crack surface. They are square with side length $5 \cdot 10^{-4}h$. The elements outside this prospective process region are modelled as linearly elastic elements. The size of these elements can thus be chosen only with regard to the numerical accuracy wanted.

2.3. Boundary conditions and symmetry

Due to the symmetry in loading and geometry, only the upper half of the body shown in Fig. 3, needs to be considered in the simulations. Along boundaries, *I*, *II* and *V*, the tractions are zero. The boundary region *IV* is loaded by the crack face pressure p. Along the symmetry line in front of the crack (region III) the symmetry conditions

$$u_y = 0,$$

$$\frac{\partial u_x}{\partial y} = 0 \tag{2}$$

are imposed, u_x and u_y denote the displacements in the horizontal and vertical directions respectively.

2.4. Solution technique

The problem is solved with a finite element code developed specially for the present investigation. The discretization in time is attained with the explicit central difference method [15]. A lumped mass matrix is used, implying that no factorization is necessary during the time stepping procedure. Four-node plane stress elements with two displacement degrees of freedom at every node are used. Since the softening behaviour, which arises from the opening of the assumed defects, is modelled with a quite general damage law (cf. (1)), the choice of one of the simplest types of elements in this region probably does not imply any severe restriction. The advantage of choosing elements with comparatively few degrees of freedom is, of course, that smaller elements can be chosen at a given computational effort. This type of element is also used for the rest of the model. In this way transition regions between elements of different types are avoided. It also simplifies the calculations, since only one type of stiffness matrix needs to be stored and used.

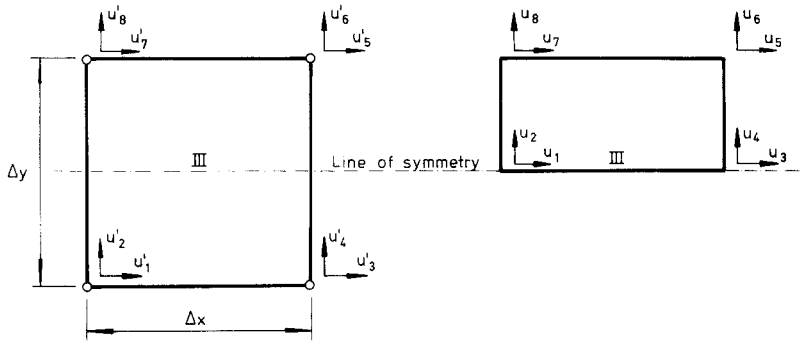

Fig. 4. (a) The displacement degrees of freedom for the full-sized elements across the line of symmetry (cf. Fig. 3). (b) The displacement degrees of freedom for the half-sized elements at the line of symmetry.

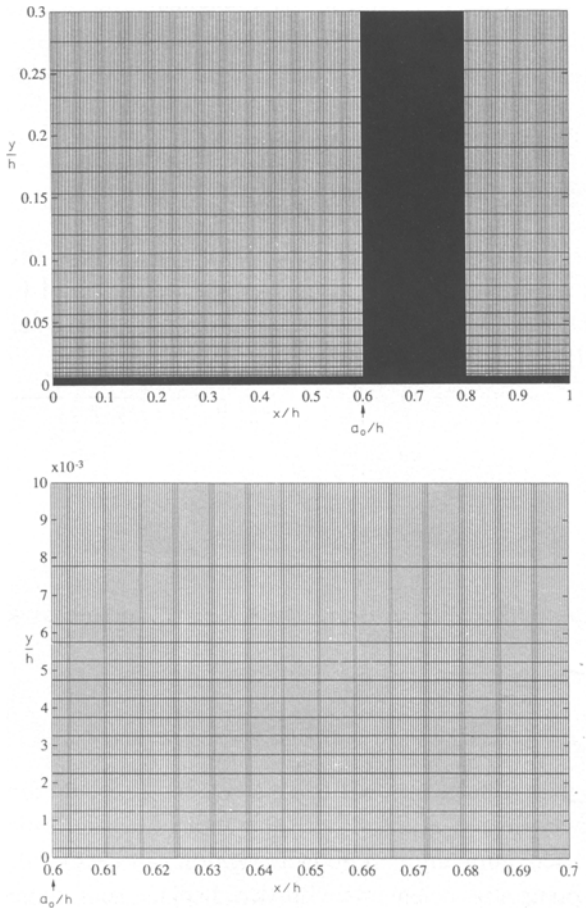

Fig. 5. The mesh used in the simulations. The initial crack tip position is located at $x = a_0$. The prospective process region occupies $0.60h \leqslant x \leqslant 0.80h$ and $0 \leqslant y \leqslant 0.006h$. In this region the elements are square-sized with side length $5.0 \cdot 10^{-4}h$. The total number of degrees of freedom is approximately 44000.

The mesh influence and the choices of certain numerical parameters controlling the accuracy of the program have been investigated and the results are given in a separate report [16]. The lowest element row consists of half-size elements which are obtained from an imagined row of full-size elements placed symmetrically around the boundary *III* as shown in Fig. 4a. For the

full-size elements the symmetry conditions imply $u'_1 = u'_7$, $u'_3 = u'_5$, $u'_2 = -u'_8$ and $u'_4 = -u'_6$. The half-size elements are generated by the upper half of the full-size elements (Fig. 4b). For these elements, therefore, $u_1 = u'_7$, $u_2 = 0$, $u_3 = u'_5$, $u_4 = 0$, $u_5 = u'_5$, $u_6 = u'_6$, $u_7 = u'_7$ and $u_8 = u'_8$. The condition $\partial u_x/\partial y = 0$ is thus approximated by a difference expression over the height of one half element. The stiffness of these elements is modified to correspond to the stiffness of the upper half of the full-size elements. Crack propagation is brought about by the succession of elements reaching $v = v_2$, i.e. by successively vanishing elements and not by change of boundary conditions.

The mesh used is shown in Fig. 5.

3. Output data

The current crack tip position $x = a$ is defined as the rightmost element in an unbroken row of vanished elements. This position is recorded at every time step and the crack tip velocity is extracted from the slope of the relation between the crack tip position and time.

Since small scale yielding prevails, the energy release rate $\mathcal{G}$ at crack length a is calculated as the sum of the energy dissipated in all cells, and summed over all time increments occuring during this crack tip position. The contribution to $\mathcal{G}$ from one specific cell during one time increment Δt consists of two parts. One part originates from the energy received by the cell during the time increment Δt, and the other part consists of the change of energy (during this time increment) that is recoverable if the cell is completely unloaded. Thus,

$$\mathcal{G} = \sum_{i=1}^{8}\sum_{j=1}^{8} \frac{\omega(v(t))k_{ij}u_i(t)(u_j(t) - u_j(t-\Delta t))}{\tau \cdot \Delta a} - \sum_{i=1}^{8}\sum_{j=1}^{8} \frac{(\tfrac{1}{2}\omega(v(t))k_{ij}u_i(t)u_j(t))}{\tau \cdot \Delta a}$$
$$+ \sum_{i=1}^{8}\sum_{j=1}^{8} \frac{(\tfrac{1}{2}\omega(v(t-\Delta t))k_{ij}u_i(t-\Delta t)u_j(t-\Delta t))}{\tau \cdot \Delta a}, \tag{3}$$

where the sums over i and j range over the eight degrees of freedom of the cell and k_{ij} is the elastic element stiffness matrix of the cell considered. The parameter Δa is the length of the process region cells in the horizontal direction. The arbitrary thickness τ is taken as the value $0.00952h$ when presenting results of $\mathcal{G}$. This value is valid for the specimen used by Ravi-Chandar, and so, a direct comparison with the experimental results shown in Figs. 1 and 2 is easily made.

4. Results

Results for different pressures p on the crack surfaces will be presented. For the first material model the choices $v_1 = 0.0020$, $v_2 = 0.048$ and $n = 1.0$ were made. This choice corresponds to the uniaxial force-displacement relation shown in Fig. 6. The responses for load magnitudes $p/E = 1.0 \cdot 10^{-3}$, $3.0 \cdot 10^{-3}$, $5.0 \cdot 10^{-3}$ and $7.0 \cdot 10^{-3}$ were investigated.

Elements that have been subjected to softening and possibly also vanishing at a time towards the end of the simulation are shown in Fig. 7. One notices that the process region expands more rapidly in the y-direction at the higher loads. The positions of softening and vanishing cells in the x-direction are shown against time in Fig. 8.

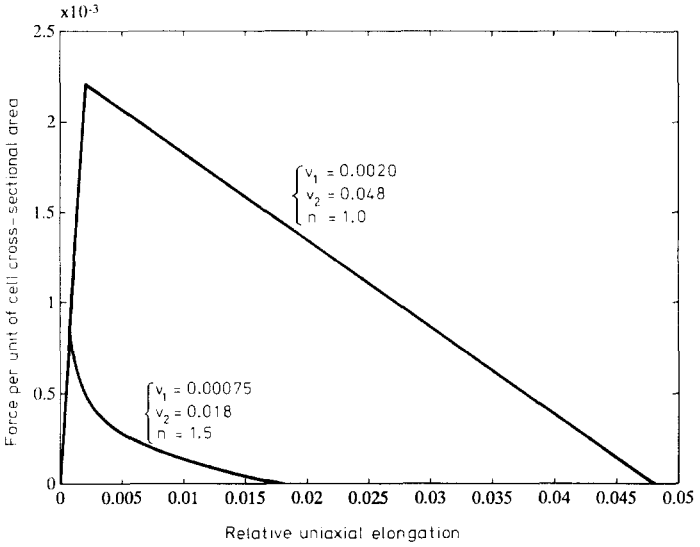

Fig. 6. The relation between force per unit of cell cross-sectional area, normalized with Young's modulus, and relative uniaxial elongation for the cells in the prospective process region. The curves are calculated for the specific case when the cell is locked to deformations in the horizontal direction.

For $p/E = 1.0 \cdot 10^{-3}$ initiation of crack growth occurs at $c_d t/h = 0.20$, see Fig. 8a. The crack accelerates to a velocity of about $0.16c_d = 0.29c_R$ at the end of the simulation, apparently without reaching a constant terminal velocity. For $p/E = 3.0 \cdot 10^{-3}$ there is an acceleration phase during a time $c_d t/h = 0.7$–0.12 followed by a constant terminal velocity of $0.24c_d = 0.44c_R$. For $p/E = 5.0 \cdot 10^{-3}$, no acceleration phase is observed and the velocity recorded, $0.22c_d = 0.41c_R$, is thus the terminal velocity. Initiation occurs at $c_d t/h = 0.05$. The remarkable result that the terminal velocity is somewhat lower than for $p/E = 3.0 \cdot 10^{-3}$ might be attributed to stronger shielding from the peripheral parts of the process region (cf. the discussion on the *barrier effect* in [4]). At further increase of the pressure to $p/E = 7.0 \cdot 10^{-3}$, the same crack velocity as for $p/E = 5.0 \cdot 10^{-3}$ is observed, whereas initiation occurred somewhat earlier, at $c_d t/h = 0.04$. It is to be noticed, however, that the latter simulation is not valid for $c_d t/h \geqslant 0.15$, or equivalently $a/h \geqslant 0.625$ since the process region height is about to overshoot the upmost one of the twelve element rows modelled as cells; see Fig. 7d.

The energy release rate against crack length can be seen in Fig. 9. One notices that the increase of energy release rate with crack length is much stronger at higher than at lower load magnitudes. At the lowest load it is constant; this is not surprising, since the extension of the process region stays approximately constant during the simulation, cf. Fig. 7a. At higher loads the crack seems to choose to dissipate excess energy in the process region rather than using it to increase its velocity.

Another simulation was performed with $v_1 = 0.00075$, $v_2 = 0.018$ and $n = 1.5$. This choice corresponds to the uniaxial force-displacement relation shown in Fig. 6. The load magnitudes $p/E = 0.3 \cdot 10^{-3}$, $1.0 \cdot 10^{-3}$, $2.0 \cdot 10^{-3}$ and $3.0 \cdot 10^{-3}$ were investigated. Figure 10 shows the rows of cells softening and vanishing against crack length. For the lowest load magnitude only the lowest cell row was subjected to softening and vanishing. The height of the process region oscillates in the last two of these simulations. This activity seems to be stronger at the higher load. For $p/E = 1.0 \cdot 10^{-3}$ and $2.0 \cdot 10^{-3}$ vanishing elements appear only in the first row.

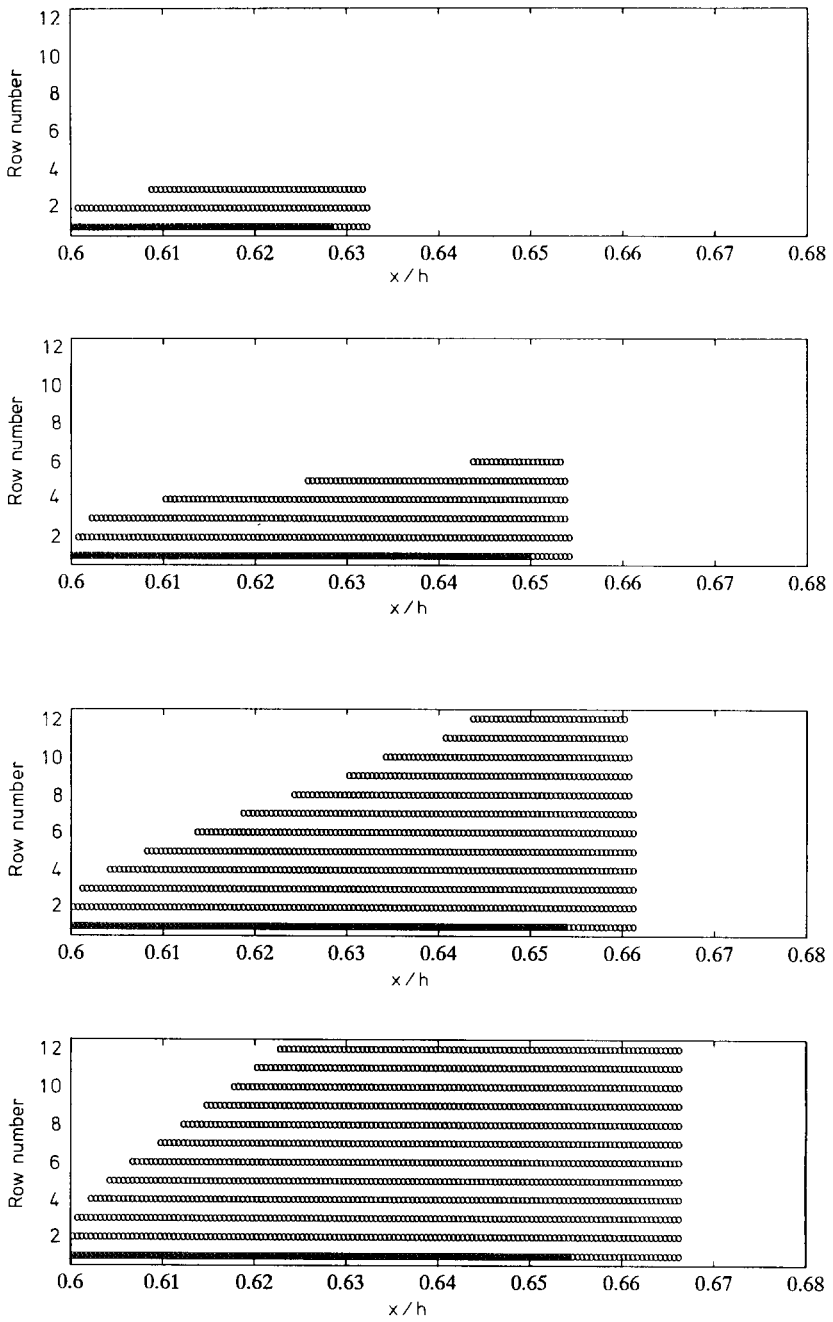

Fig. 7. Elements in the different cell rows which have reached the softening state (o) and the vanishing state (x) are shown against their x-position at a time towards the end of the simulations. Four different load cases are considered: p/E = (a) $1.0 \cdot 10^{-3}$, (b) $3.0 \cdot 10^{-3}$, (c) $5.0 \cdot 10^{-3}$ and (d) $7.0 \cdot 10^{-3}$. $v_1 = 0.0020$, $v_2 = 0.048$ and $n = 1.0$.

The case $p/E = 3.0 \cdot 10^{-3}$ shows an attempted branching at $x/h = 0.61$, see Fig. 10d. In fact, only the branch is propagated for a while, but then the main crack again starts to propagate straight forward. Thereupon the branch becomes arrested. Another attempted branching at $x/h = 0.645$ also fails. At $x/h = 0.665$ successful branching is initiated. Even though softening

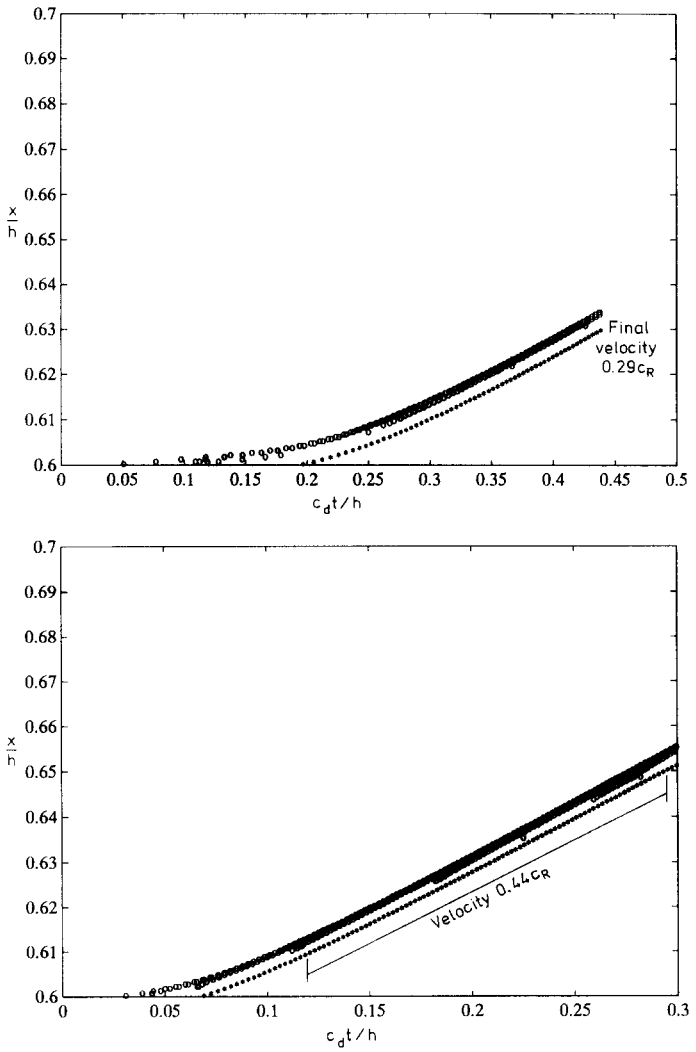

Fig. 8. The x-coordinate against time for all elements that have reached the softening state (o) and the vanishing state (*) at a time towards the end of the simulation. The pressure on the crack surfaces is p/E = (a) $1.0 \cdot 10^{-3}$, (b) $3.0 \cdot 10^{-3}$, (c) $5.0 \cdot 10^{-3}$ and (d) $7.0 \cdot 10^{-3}$. The islands of softening in (c) are due to some elements behind the crack tip reaching the softening state. The crack velocities are shown in the figures. $v_1 = 0.0020$, $v_2 = 0.048$ and $n = 1.0$.

has occurred several times in the twelfth element row, the results are believed to be approximately valid until about $c_d t/h = 0.28$ when the successful branch tends to overshoot the twelfth row.

The x-positions of softening and vanishing elements against time are shown in Fig. 11. The increased activity at increased load gives a less smooth crack length variation with time. The velocities seem to increase with increasing load magnitude. For $p/E = 0.3 \cdot 10^{-3}$ no terminal velocity seems to be approached, and the velocity reaches its highest value, $0.20c_d = 0.37c_R$, at the end of the simulation. At the higher loads constant terminal velocities, approximately $0.30c_d = 0.55c_R$ at $p/E = 1.0 \cdot 10^{-3}$, $0.31c_d = 0.58c_R$ at $p/E = 2.0 \cdot 10^{-3}$ and $0.33c_d = 0.61c_R$ at $p/E = 3.0 \cdot 10^{-3}$, are reached rather soon after the initiation of crack propagation.

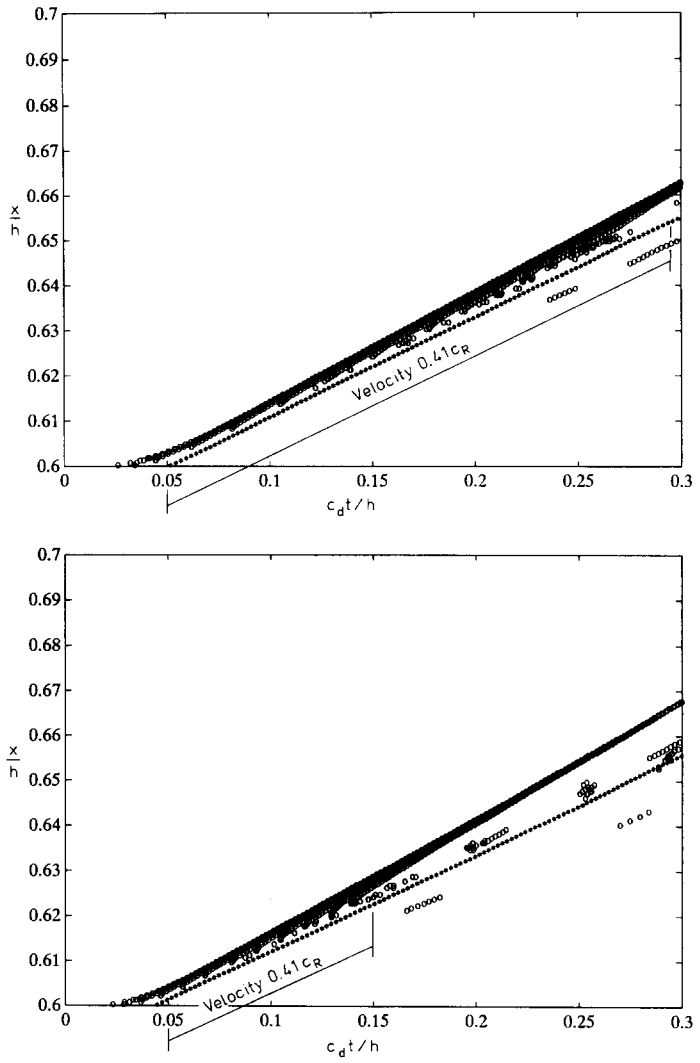

Fig. 8 (cont.)

The energy release rates along the crack paths can be seen in Figs. 12. As could be expected, the energy release rate is rather constant for the two lowest loads. For $p/E = 2.0 \cdot 10^{-3}$ it is on the average rather constant except for large peaks in regions with process region peaks. For the highest load such peaks are present at the branching trials. In this case the average energy release rate increases significantly with the crack length.

Several simulations with other combinations of the model parameters v_1, v_2 and n have been performed; they are reported in [16]. The main result seems to be that a lower value of v_1 implies larger length and height of the process region, a shorter time of crack acceleration and a higher terminal velocity. A lower value of v_2 implies a shorter process region, a slightly shorter time of crack acceleration and a slightly higher terminal velocity. The influence of v_1 and v_2 on the tendency for branching is more complicated. For a given load, a given size of the model and a given value of n it seems to be necessary to have a sufficiently low value of v_1 and a value of v_2 that is neither too large nor too small to get crack branching with a certain time of simulation. A

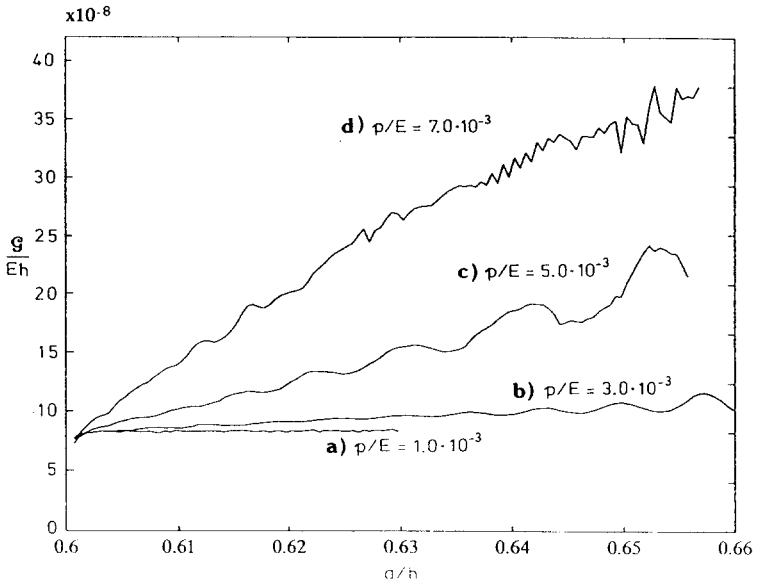

Fig. 9. The energy release rate $\mathcal{G}$ against crack length for the four different pressure magnitudes p/E = (a) $1.0 \cdot 10^{-3}$, (b) $3.0 \cdot 10^{-3}$, (c) $5.0 \cdot 10^{-3}$ and (d) $7.0 \cdot 10^{-3}$. $v_1 = 0.0020$, $v_2 = 0.048$ and $n = 1.0$.

lower value of n seems to increase the height of the process region and to reduce the terminal velocity as well as the tendency for branching.

Simulations with different cell sizes in the prospective process region were investigated for fixed v_1, v_2, n and p. No dramatic changes were observed when reducing the cell size, but the

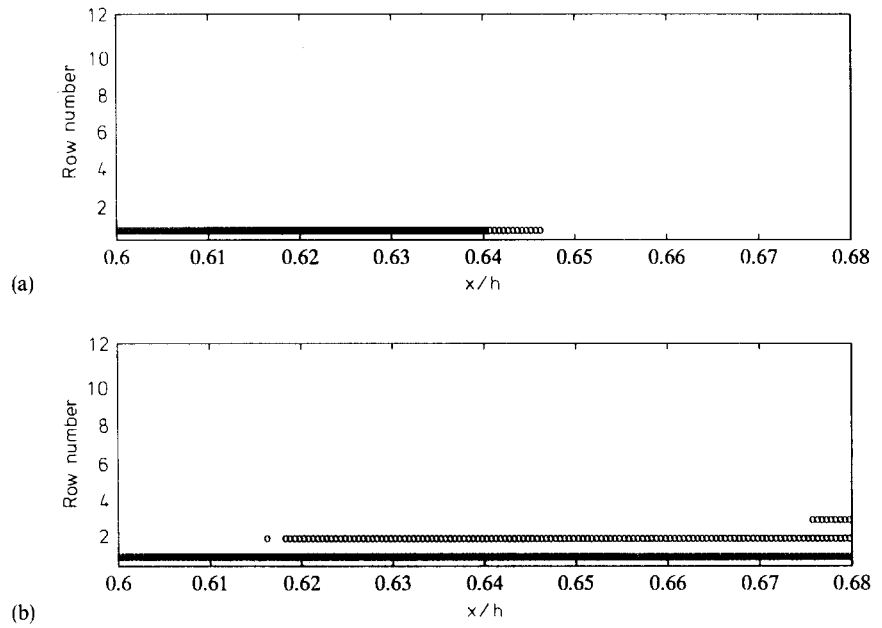

Fig. 10. Elements in the different cell rows which have reached the softening state (o) and the vanishing state (x) are shown against their x-position at a time towards the end of the simulations. The load magnitudes are p/E = (a) $0.3 \cdot 10^{-3}$, (b) $1.0 \cdot 10^{-3}$, (c) $2.0 \cdot 10^{-3}$ and (d) $3.0 \cdot 10^{-3}$. $v_1 = 0.00075$, $v_2 = 0.018$ and $n = 1.5$.

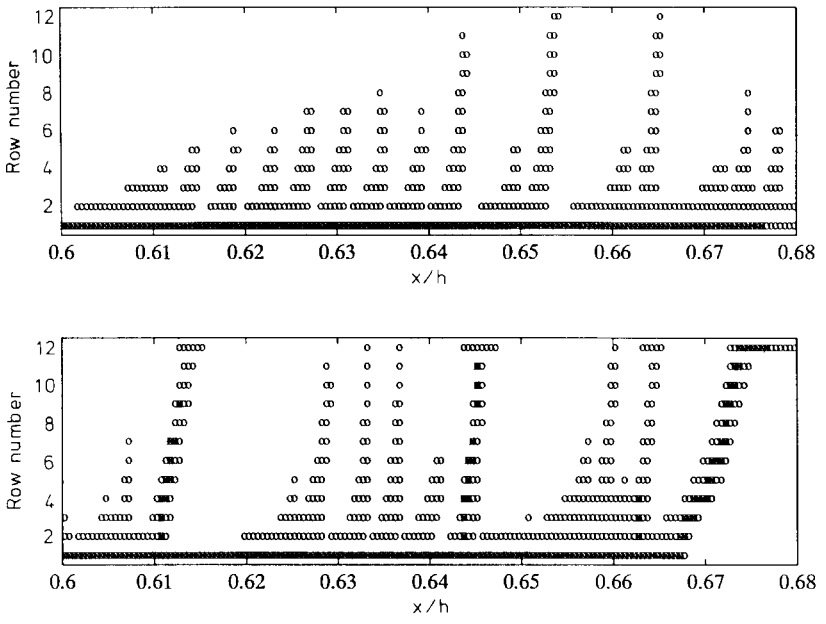

Fig. 10. (cont.)

softening and vanishing activity along the crack path is increased and both attempted and successful branching occur earlier.

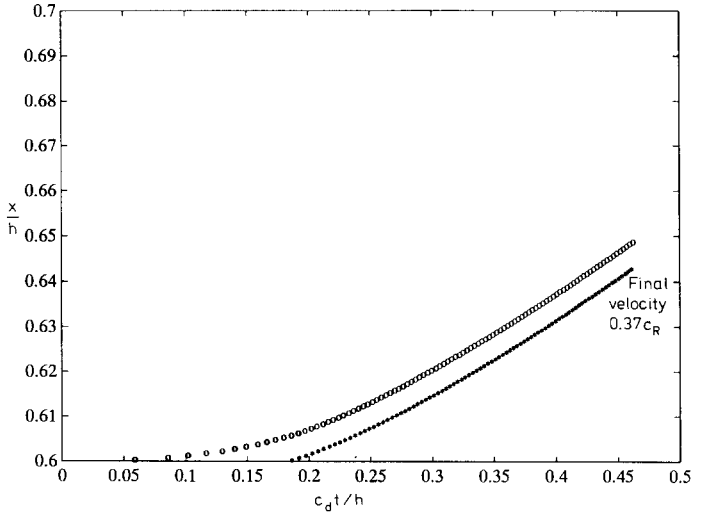

Fig. 11. The x-coordinate against time for all elements that have reached the softening state (o) and the vanishing state (*) at a time towards the end of the simulation. The pressure on the crack surfaces is p/E = (a) $0.3 \cdot 10^{-3}$, (b) $1.0 \cdot 10^{-3}$, (c) $2.0 \cdot 10^{-3}$ and (d) $3.0 \cdot 10^{-3}$. The crack velocities are indicated in Fig. 11a and Fig. 11b. An irregular, but over large distances approximately constant terminal velocity is reached for the two highest loads. It is estimated to $0.58c_R$ in Fig. 11c and to $0.61c_R$ in Fig. 11d. $v_1 = 0.00075$, $v_2 = 0.018$ and $n = 1.5$.

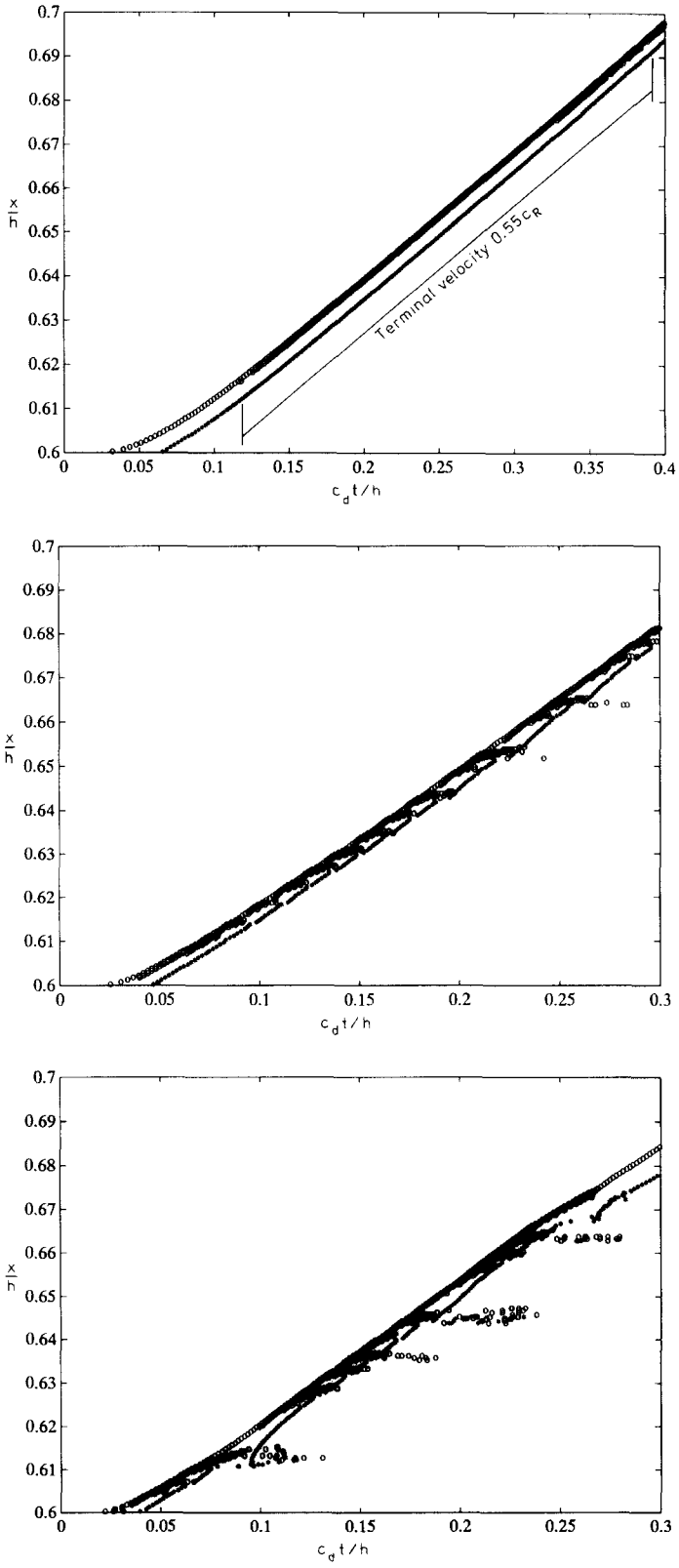
0.7
0.69
0.68
0.67
0.66
0.65
0.64
0.63
0.62
0.61
0.6
x/L
Terminal velocity 0.55c_R
0
0.05
0.1
0.15
0.2
0.25
0.3
0.35
0.4
c_d t/h

Fig. 11. (cont.)

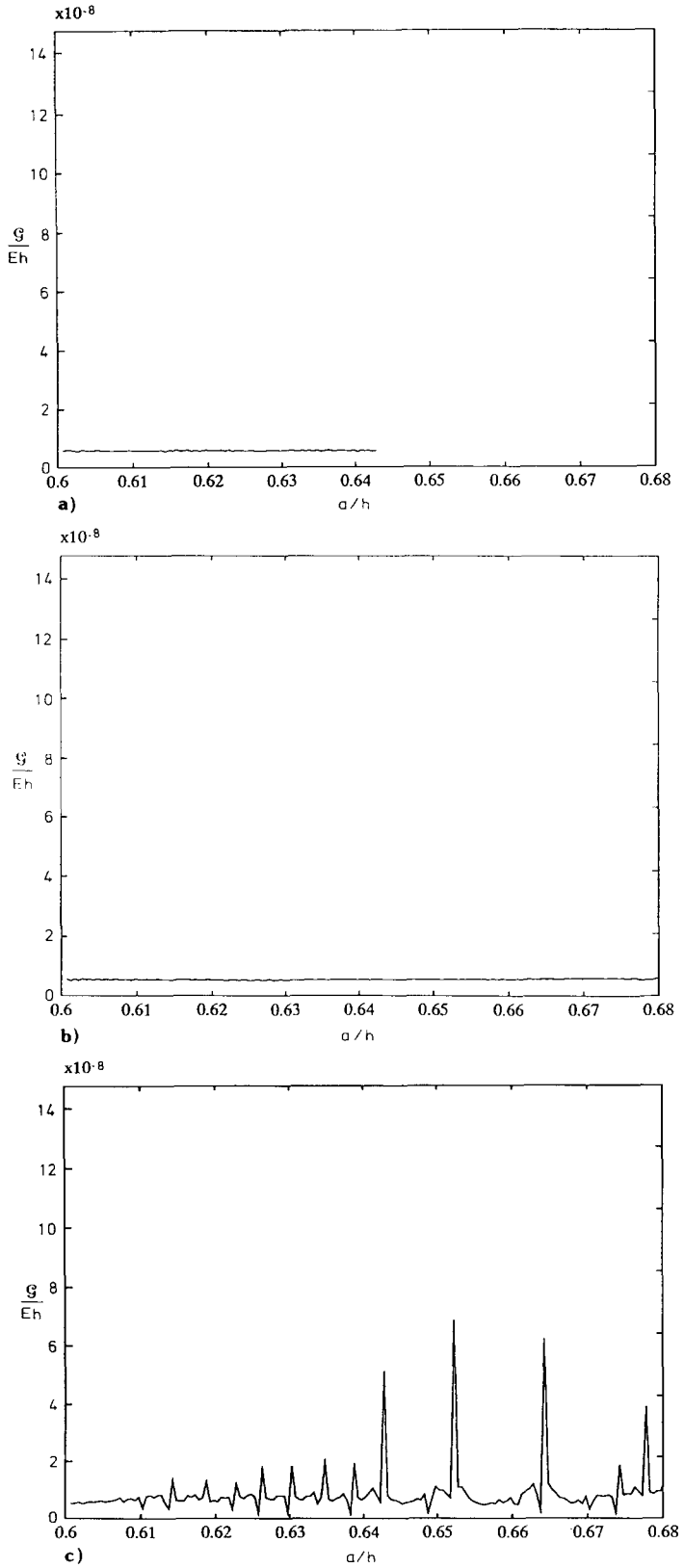

Fig. 12. The energy release rate $\mathcal{G}$ against crack length for the four different crack surface pressures p/E = (a) $0.3 \cdot 10^{-3}$, (b) $1.0 \cdot 10^{-3}$, (c) $2.0 \cdot 10^{-3}$ and (d) $3.0 \cdot 10^{-3}$. $v_1 = 0.00075$, $v_2 = 0.018$ and $n = 1.5$.

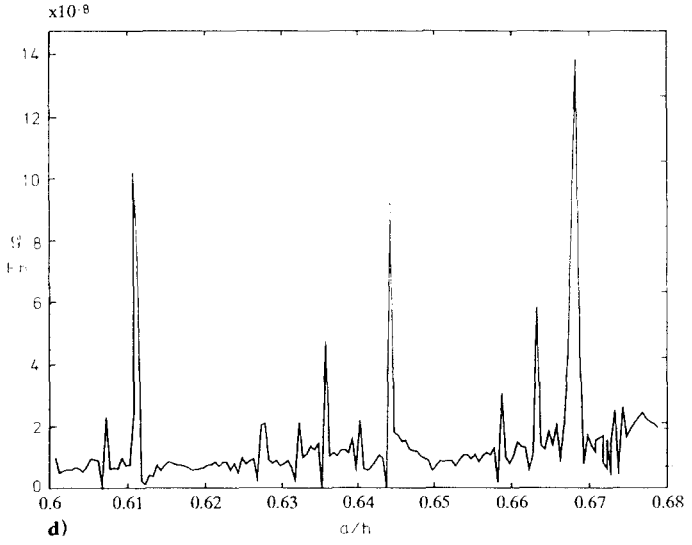

Fig. 12. (cont.)

5. Discussion and conclusion

By using a cell model for the process region it has been possible to simulate some noteworthy, recently experimentally detected properties of rapid crack growth. Quite in agreement with these findings, a constant terminal velocity was obtained for the high velocity region at the same time as the energy release rate increased considerably during crack growth. A comparison between, for instance, the simulated results shown in Figs. 8 and 9 and the experimental results reproduced in Figs. 1 and 2, show a striking resemblence, even as regards the magnitude of the constant terminal velocity at the higher loads. A peculiar phenomenon was detected, viz., that the terminal velocity in one set of simulations was slightly lowered at an increase of the load; this phenomenon was attributed to shielding. In some cases, especially at high velocities, attempts to branching and even successful branching were obtained. The observation that several attempts of branching preceded successful branching is in agreement with experimental and theoretical results mentioned in the Introduction.

Present knowledge about process properties is not sufficient to give guidelines about the choice of the parameters v_1, v_2 and n for different materials. It was found that different combinations lead to different propensity towards branching and to different magnitudes of the terminal velocities. This is not an unexpected result: on the contrary, it is known that different materials show quite different behaviour in these respects. It should also be remembered that the material model used is considerably idealized: no viscoplastic flow or other rate dependent properties have been incorporated for the process region or for the continuum outside this region. Nevertheless the results appear to confirm the anticipation that the properties of the process region constitute the main factor responsible for the lack of a unique relation between energy release rate and crack edge velocity in the high velocity region. Studies of the process

region morphology obtained in the simulations also clearly show that there is no unique relation between the cell size and the process region height. This confirms the anticipation [4], [5] that the control of the process region by an intrinsic length parameter gets lost at very high velocities.

Acknowledgments

The author is sincerely grateful to Professor K.B. Broberg for several interesting and invaluable discussions and for his support during the course of this work. Thanks also to Ms. D. Nilsson for drawing the figures.

References

1. A.A. Griffth, *Philosophical Transactions of the Royal Society* (London) A221 (1920) 163–198.
2. G.R. Irwin, *Journal of Applied Mechanics* 24 (1957) 361–364.
3. T.L. Paxson and R.A. Lucas, *Proceedings of an International Conference on Dynamic Crack Propagation, Lehigh University, Bethlehem, Pennsylvania, USA*, Nordhoff International Publishing, Leyden (1972) 415–426.
4. K.B. Broberg, in *High Velocity Deformation of Solids, IUTAM, Tokyo, August 24–27 1977*, Springer-verlag, Berlin (1977) 182–194.
5. K.B. Broberg, in *Fundamentals of Deformation and Fracture*, Cambridge University Press (1985) 233–242.
6. K. Ravi-Chandar, *Doctoral thesis*, California Institute of Technology, Pasadena (1982).
7. K. Ravi-Chandar and W.G. Knauss, *International Journal of Fracture* 25 (1984) 247–262.
8. K. Ravi-Chandar and W.G. Knauss, *International Journal of Fracture* 26 (1984) 65–80.
9. K. Ravi-Chandar and W.G. Knauss, *International Journal of Fracture* 26 (1984) 141–154.
10. K. Ravi-Chandar and W.G. Knauss, *International Journal of Fracture* 26 (1984) 189–200.
11. J.F. Kalthoff, S. Winkler and J. Beinert, *International Journal of Fracture* 12 (1976) RCR 317–319.
12. J.F. Kalthoff, in *Workshop on Dynamic Fracture*, February 17–18, California Institute of Technology (1983) 11–35.
13. K.B. Broberg, *Engineering Fracture Mechanics* 16 (1982) 497–515.
14. L.G. Pärletun, *Engineering Fracture Mechanics* 11 (1979) 343–358.
15. T. Belytschko and T. Hughes, *Computational Methods for Transient Analysis*, Elsevier, Amsterdam (1983).
16. E. Johnson, Influence of process region characteristics on rapid crack propagation, Report LUTFD2/(TFHF-3043), Solid Mechanics, Lund Institute of Technology, Lund (1991).